Al-Turath Journal for Biology (ATJB)
Open Access Journal
Open Access Journal
ISSN Print: 3080-1265
Online : 3080-1273

Original Paper

Spatial assessment of the ecological hazards of polycyclic aromatic hydrocarbons (PAHs), total petroleum hydrocarbons (TPHs), and soil thermal footprint. Fallujah, Iraq

Omar Ali Jasim
Al-Siraj Private University College of Science, Forensic Science Department
Correspondence email | dr.omar8ali@gmail.com
Received: 18/01/2026 | **Accepted**: 08/03/2026 | **Available online:** 31/03/2026 | **DOI:** https://doi.org/10.63964/atjb.2026.1.3

ABSTRACT
Post-conflict environments in Iraq, and Fallujah (Anbar Governorate) in particular, have been subjected to repeated high-intensity military operations, widespread building demolition, open burning of infrastructure, and fuel-depot destruction, all of which are known to deposit pyrogenic polycyclic aromatic hydrocarbons (PAHs) and petroleum hydrocarbons (TPH) into adjacent agricultural soils. Despite an internationally recognised legacy of environmental and health concern in Fallujah, comprehensive organic soil contamination datawith spatial resolution, quantitative risk assessment, and soil-quality indexing remain scarce in the peer-reviewed literature. **Objectives:** To determine the concentrations of the 16 USEPA priority PAHs, total petroleum hydrocarbons (TPH C10–C40), benzo[a]pyrene toxic equivalent quotient (BaP-TEQ), and black carbon (BC) across a twelve-site spatial network in Fallujah; to compute the Pollution-Load Index (PLI), Contamination Factor (CF), and Integrated Soil-Quality Index (SQI); to identify PAH sources using diagnostic ratios and principal component analysis (PCA); to characterise the spatial decay from the conflict epicentre; and to assess ecotoxicological and human-health implications against international soil-screening standards. **Methods:** Twelve surface soil samples (0–20 cm) were collected from sites spanning 120–2,850 m from the Al-Sarai conflict epicentre in November 2023 dry season to minimise leaching bias. Σ_{16}PAHs and individual congeners were quantified by GC-MS (SIM mode; deuterated surrogate internal standards; seven-point calibration; MDL 0.005 µg/mL); TPH (C10–C40) by GC-FID (ISO 16703; nine-point calibration); black carbon (BC) by thermo-optical analysis (EUSAAR_2 protocol). Physicochemical parameters (pH, EC, TOC, CEC, TN, available P, $CaCO_3$) were determined by standard methods. Contamination indices (CF, PLI, BaP-TEQ), source fingerprinting (diagnostic ratios; Fla/(Fla+Pyr); Ant/(Ant+Phe); IcdP/(IcdP+BghiP); BaA/(BaA+Chr)), PCA, ordinary-kriging interpolation, and Spearman/Pearson correlations were computed. Spatial decay modelling used nonlinear least-squares exponential fitting. **Results:** Σ_{16}PAH ranged from 0.24 mg/kg (background, S-12) to 16.56 mg/kg (epicentre, S-01), with extreme contamination (> 10 mg/kg; Maliszewska-Kordybach class IV) at three sites within 220 m of the epicentre. BaP-TEQ peaked at 4.97 mg/kg at S-01, exceeding the 1.0 mg/kg indicative action level at three sites. TPH peaked at 3,079 mg/kg (S-01) versus a background of 105 mg/kg; the Dutch TPH target value (50 mg/kg) was exceeded at nine of twelve sites. The integrated organic PLI reached 14.75 at S-01; ordinary-kriging surfaces show PLI > 3 (highly polluted) persisting to ≈ 400 m and PLI > 2 to ≈ 600 m from the epicentre. Exponential spatial-decay modelling estimated half-distances of 333 m (Σ_{16}PAH) and 276 m (BaP-TEQ). PCA (PC1 = 92.4% variance) and diagnostic ratios (Ant/(Ant+Phe) > 0.10; Fla/(Fla+Pyr) > 0.50) confirmed a dominantly pyrogenic combustion source at epicentre and high-tier sites. SQI was severely impaired at the three extreme sites (SQI ≤ 0.072 vs background 0.90). **Conclusions:** Fallujah agricultural soils within ≈ 400 m of the Al-Sarai conflict epicentre are severely contaminated with carcinogenic pyrogenic PAHs and petroleum hydrocarbons, with organic PLI values exceeding all published Iraqi and regional benchmarks. The SQI data confirm concurrent biological soil function impairment. These findings provide a spatial, multi-parameter evidence base for prioritised remediation, agricultural land-use restrictions within the extreme tier, and continued environmental health monitoring in Fallujah as mandated by UN Environment Programme principles for post-conflict recovery.

KEYWORDS: *polycyclic aromatic hydrocarbons; soil quality index; Iraq; pollution-load index; organic pollutants*

1-INTRODUCTION

Fallujah, located on the Euphrates River approximately 69 km west of Baghdad in Anbar Governorate, Iraq, was the site of two of the most intense urban combat operations of the post-2003 Iraq conflict , Operations Vigilant Resolve (April 2004) and Phantom Fury (November–December 2004) followed by sustained conflict during the 2014–2016 period of ISIL control and subsequent liberation operations [1,2]. These operations involved heavy artillery bombardment, aerial ordnance deployment, thermobaric munitions, armoured vehicle fuel destruction, and widespread structural demolition, collectively releasing large quantities of combustion by-products including pyrogenic polycyclic aromatic hydrocarbons (PAHs) and petroleum-derived hydrocarbonsinto the surrounding environment [1,3]. The legacy of this contamination is compounded by the destruction of fuel depots, military

https://doi.org/10.63964/atjb.2026.1.3

vehicle scrappage, and prolonged smouldering of rubble in close proximity to agricultural land on the city's periphery [2,4].

Polycyclic aromatic hydrocarbons (PAHs) are a class of persistent organic pollutants (POPs) formed primarily through incomplete combustion of organic matter and fossil fuels. The sixteen congeners designated as priority pollutants by the US Environmental Protection Agency (USEPA) include several well-documented human carcinogens notably benzo[a]pyrene (BaP; IARC Group 1), dibenz[a,h]anthracene (DahA; IARC Group 2A), and indeno[1,2,3-cd]pyrene (IcdP; IARC Group 2B) [5,6]. In soils, PAHs sorb strongly to organic matter and black carbon, making them highly persistent with environmental half-lives of months to decades depending on the molecular weight of the congener and soil redox conditions [5,7]. Total petroleum hydrocarbons (TPH; C10–C40) co-occur with PAHs at fuel-contaminated sites and contribute independently to phytotoxicity, soil microbial community disruption, and human dermal/ingestion exposure [8]. Black carbon (BC) the particulate carbonaceous product of incomplete combustion serves both as a PAH-sorbing matrix that modulates bioavailability and as an independent tracer of pyrogenic input intensity [7].

Despite mounting international concern over the environmental and public-health legacy of conflict in Iraq, peer-reviewed data on soil organic contamination from Fallujah are extremely sparse. Al-Azzawi and colleagues (2012) reported elevated PAHs in Fallujah urban soils, predominantly from traffic and open burning, but predated the 2014–2016 period of most intense urban destruction and did not compute composite risk indices [9]. International health studies have documented elevated rates of birth defects, childhood cancers, and haematological disorders in Fallujah compared with pre-conflict baselines and with other Iraqi cities [2,3], though environmental exposure data linking these outcomes to specific soil contaminants are lacking. The UN Environment Programme (UNEP) has called for systematic post-conflict environmental assessment in Iraq as a prerequisite for sustainable reconstruction and agricultural recovery [4], yet government and academic capacity for such assessments has been severely constrained by resource limitations.

The selection of appropriate contamination indices is critical for translating analytical soil chemistry data into decision-relevant risk categories. The Maliszewska-Kordybach (1996) PAH classification system provides ecotoxicologically grounded threshold bands specifically validated against soil biological endpoint data [8]. The Pollution-Load Index (PLI) computed as the geometric mean of normalised contamination factors for multiple analytes provides a composite measure of overall organic pollution pressure calibrated to background concentrations [9]. The Contamination Factor (CF) quantifies how far each analyte exceeds its geochemical background at each site, enabling spatial prioritisation. The Integrated Soil-Quality Index (SQI) synthesises a suite of physicochemical and fertility indicators into a single dimensionless score (0–1) that captures the functional integrity of the soil system [10]. Together, these indices convert a multi-analyte dataset into a coherent spatial risk map that can guide remediation prioritisation, agricultural land-use zoning, and community health-protection measures.

The present study provides the first post-2016 comprehensive GC-MS/GC-FID organic contamination assessment of Fallujah agricultural soils with: (i) spatial coverage spanning 120–2,850 m from the Al-Sarai conflict epicentre; (ii) quantification of all 16 USEPA priority PAHs, TPH, and black carbon; (iii) pyrogenic source fingerprinting by diagnostic ratios and PCA; (iv) computation of BaP-TEQ, PLI, CF, and SQI across all twelve sites; (v) spatial decay modelling and ordinary-kriging contamination mapping; and (vi) assessment against WHO, USEPA, and Dutch soil-quality standards. The results are intended to support evidence-based remediation planning and agricultural policy for Fallujah's post-conflict environmental recovery.

2. MATERIALS AND METHODS

2.1 Study area and site selection: The study area comprises agricultural and peri-urban land within and around Fallujah city (33°21'N, 43°46'E), Anbar Governorate, western Iraq. Twelve sampling sites (S-01 to S-12) were established along four transects radiating from the Al-Sarai district the documented epicentre of heaviest conflict damage spanning distances of 120 to 2,850 m from this reference point (Table 1; Figure 2). Sites were categorised a priori into four conflict-exposure tiers based on published conflict damage mapping [1,2]: Extreme (S-01, S-06, S-08; < 300 m); High (S-02, S-09, S-11; 300–500 m); Moderate (S-04, S-05, S-10; 500–1,500 m); Background (S-03, S-07, S-12; > 2,000 m). Background sites were selected to represent pre-conflict agricultural baseline conditions based on absence of structural damage and local soil-survey records predating 2004.

2.2 Sample collection and preparation: Surface soil samples (0–20 cm depth; composite of five sub-samples per site collected in an X pattern from a 10×10 m plot) were collected in pre-cleaned amber glass jars during November 2023 (dry season; avoiding post-rain leaching bias). In situ measurements of surface temperature, moisture content, and GPS coordinates (WGS-84, ±2 m accuracy) were recorded. Samples were immediately placed in cool boxes (4°C) and transported to the Soil and Environmental Chemistry Laboratory, University of Anbar, within 6 hours. On receipt, samples were spread on clean aluminium trays and air-dried at room temperature (22°C) for 72 hours, sieved through a 2-mm stainless-steel mesh, homogenised, and stored at −20°C until analysis. All glassware was pre-cleaned by sequential washing with laboratory-grade detergent, tap water, deionised water, acetone, and dichloromethane before use; field blanks (clean sand) and lab procedural blanks were processed alongside samples.

2.3 Physicochemical characterization: Soil pH and electrical conductivity (EC) were measured in a 1:2.5 (w/v) soil:deionised-water suspension using calibrated Mettler-Toledo pH and EC probes. Soil organic carbon (SOC) was determined by the Walkley-Black wet oxidation method; total nitrogen (TN) by the Kjeldahl method; available phosphorus (Av-P) by the Olsen method ($NaHCO_3$ extractant; colorimetric measurement at 882 nm). Cation exchange capacity (CEC) was determined by ammonium acetate saturation (pH 7.0). Calcium carbonate ($CaCO_3$) equivalent was measured by the calcimeter (Bernard) method. Bulk density (BD) was determined from undisturbed core samples using the core method; textural analysis (sand, silt, clay) by the hydrometer method (ASTM D7928). Black carbon (BC) was determined by the thermo-optical transmittance (TOT) method using a Sunset Laboratory OC/EC analyser, EUSAAR_2 protocol [11].

2.4 PAH extraction and GC-MS analysis: Σ_{16}PAH extraction followed the modified EPA Method 3545A (accelerated solvent extraction; ASE): 5 g dry soil in a 33-mL ASE cell, extracted with dichloromethane:acetone (1:1 v/v) at 100°C, 1,500 psi, three static cycles of 5 minutes. Before extraction, each sample was spiked with deuterated surrogates (naphthalene-d_8, acenaphthylene-d_8, phenanthrene-d_{10}, chrysene-d_{12}, and perylene-d_{12}; 100 ng/g each) for recovery correction. Extracts were concentrated by rotary evaporation to 1 mL, solvent-exchanged to hexane, and cleaned on an Alumina/Silica SPE column (elution: 10 mL hexane then 20 mL DCM:hexane 1:4). Final extracts were spiked with 5-α-androstane as injection standard and analysed by GC-MS (Shimadzu QP2020 NX; DB-5MS column, 30 m × 0.25 mm × 0.25 µm; SIM mode; carrier gas He at 1.2 mL/min; injector 280°C; MS transfer line 290°C; temperature programme: 60°C (1 min) → 20°C/min → 180°C → 5°C/min → 290°C (15 min); typical run time 46 min). Quantification used seven-point external calibration curves (0.005–10.0 µg/mL; $r^2 \geq 0.9997$ for all congeners; Figure 1A). Mean surrogate recoveries: 78–113% (all within EPA 8270D acceptance limits of 60–125%). Method detection limits: 0.005–0.022 µg/g (PAH-congener dependent)[12].

2.5 TPH extraction and GC-FID analysis: TPH (C10–C40) was determined by GC-FID following modified ISO 16703:2004. Five grams of dry soil was extracted with n-hexane (3 × 25 mL; 30-min sonication cycles), extracts pooled, passed through anhydrous Na_2SO_4, concentrated to 1 mL and analysed on a Shimadzu GC-2010 Plus (Zebron ZB-1 column, 30 m × 0.32 mm × 0.25 µm; FID 300°C; H_2 carrier 2.0 mL/min; injector 280°C; programme: 40°C (2 min) → 10°C/min → 300°C (10 min)). Quantification against a nine-point calibration of certified mineral oil standard (5–2,000 mg/L; $r^2 = 0.99987$; Figure 1B). MDL: 5 mg/kg. Laboratory QC included duplicate analysis (relative deviation < 8%), matrix spike recovery (89–108%), and certified reference material (CRM 104 Organics in Soil, QC Lot 3310-7; recovery 96.4%) [13].

2.6 Contamination indices: The Contamination Factor (CF) for each contaminant at each site was computed as CF = C_site / C_background, where C_background was the arithmetic mean of concentrations at the two background sites (S-07, S-12) for PAH and TPH, and the national geochemical background for BC and physicochemical parameters. The Pollution-Load Index (PLI) was computed as: PLI = (CF_PAH × CF_TPH × CF_BC)^(1/3), providing a composite geometric mean. The BaP-TEQ (Toxic Equivalent Quotient) was calculated by summing the product of each PAH congener concentration and its Toxic Equivalency Factor (TEF) relative to benzo[a]pyrene (Nisbet & LaGoy, 1992) [13]: $BaP\text{-}TEQ = \Sigma(C_i \times TEF_i)$. The Integrated Soil-Quality Index (SQI) was calculated following Andrews et al. (2004) [12]: $SQI = \Sigma(w_i \times s_i)$, where w_i is the weight of indicator i (derived from PCA-explained variance) and s_i is the normalised (0–1) scoring function value for indicator [14]

2.7 Pyrogenic source fingerprinting: PAH sources were identified using four binary molecular diagnostic ratios with established source-discrimination boundaries [14]: (i) Fluoranthene/(Fluoranthene+Pyrene) [Fla/(Fla+Pyr)]: > 0.50 = pyrogenic combustion; < 0.50 = petrogenic; (ii) Anthracene/(Anthracene+Phenanthrene) [Ant/(Ant+Phe)]: > 0.10 = pyrogenic; < 0.10 = petrogenic; (iii) Indeno[1,2,3-cd]pyrene/(IcdP+Benzo[ghi]perylene)

[IcdP/(IcdP+BghiP)]: > 0.50 = combustion; (iv) BaA/(BaA+Chrysene): > 0.35 = combustion; 0.20–0.35 = mixed. These ratios were plotted as cross-plots, and principal component analysis (PCA; z-standardised data; varimax rotation) was conducted to identify the dominant variance structure across the full multi-analyte dataset [15]

2.8 Spatial analysis and statistical methods: Ordinary kriging interpolation of PLI and Σ_{16}PAH surfaces was performed in R v4.3.2 (gstat package) using a fitted spherical variogram; cross-validation was by leave-one-out (LOO) method. Spatial decay of Σ_{16}PAH and BaP-TEQ with distance from the epicentre was modelled by nonlinear least-squares (NLS) exponential decay: $C(d) = C_0 \times \exp(-k \times d)$, with half-distance $d_{1/2} = \ln(2)/k$. Pearson and Spearman correlations between contaminants and physicochemical parameters were computed in SPSS v27. Significance was set at $\alpha = 0.05$ (two-sided); corrections for multiple comparisons used the Benjamini-Hochberg false discovery rate (FDR) procedure where noted [16].

3. Results

3.1 Physicochemical soil characteristics: Soil physicochemical properties across the twelve sites are summarised in Table 2. All soils were alkaline (pH 7.88–8.35), consistent with Iraq's calcareous semi-arid soil taxonomy (Typic Torriorthents), with pH tending to be highest at epicentre-proximal sites (pH 8.29–8.35 at extreme-tier sites vs 7.88–7.97 at background sites). Electrical conductivity (EC) at extreme-tier sites (4.16–4.56 dS/m) exceeded the FAO guideline for negligible salinity impact on sensitive crops (< 2.0 dS/m) and approached the threshold for moderate restriction (> 4.0 dS/m), suggesting salinisation linked to ash deposition and structural debris leaching. Total organic carbon (TOC) was paradoxically elevated at contaminated sites (3.13–3.38%) compared with background (1.14–1.22%), reflecting the incorporation of pyrogenic carbon (black carbon fraction) rather than labile organic matter. Black carbon ranged from 0.91% (S-07 background) to 7.26% (S-08 epicentre), with the extreme tier averaging BC/TOC ratios > 0.55, indicative of a strongly pyrogenic soil organic fraction. CEC was inversely correlated with contamination tier (15.1–15.6 cmol/kg extreme vs 20.6–21.2 background), consistent with PAH/BC-mediated suppression of clay-organic charge interactions. Total nitrogen (TN) and available phosphorus (Av-P) were similarly lowest at contaminated sites, reflecting phytotoxic inhibition of nitrogen-cycling microbial communities.

Table 1. Site locations and primary contamination indices.

Site	Distance (m)	Tier	Σ_{16}PAH (mg/kg)	TPH (mg/kg)	BaP-TEQ (mg/kg)	PLI	SQI
S-01	120	Extreme	**16.56**	**3079**	4.968	**14.75**	**0.048**
S-02	310	High	**11.08**	**1889**	2.992	9.95	0.278
S-03	2100	Background	0.45	**115**	0.086	0.61	0.964
S-04	780	Moderate	4.18	**653**	0.982	3.82	0.611
S-05	1150	Moderate	2.07	**293**	0.486	2.17	0.635
S-06	180	Extreme	**13.16**	**2684**	3.948	**13.11**	**0.072**
S-07	2600	Background	0.28	**105**	0.053	0.48	0.897
S-08	220	Extreme	**12.77**	**2491**	3.831	**13.10**	**0.058**
S-09	430	High	8.12	**1452**	2.192	7.54	0.285
S-10	950	Moderate	2.83	**515**	0.665	2.87	0.584
S-11	290	High	**10.61**	**2072**	2.865	9.63	0.271
S-12	2850	Background	0.24	**107**	0.046	0.46	0.901

Distance = distance from Al-Sarai conflict epicentre (m). Σ_{16}PAH = sum of 16 USEPA priority PAHs; TPH = total petroleum hydrocarbons C10–C40; BaP-TEQ = benzo[a]pyrene toxic equivalent quotient (Nisbet & LaGoy, 1992 TEFs); PLI = Integrated Organic Pollution-Load Index; SQI = Soil-Quality Index (Andrews et al., 2004). Bold/red values exceed critical thresholds (Σ_{16}PAH > 10 mg/kg; SQI < 0.10).

Table 2. Physicochemical properties of the twelve soil samples

Site	pH	EC (dS/m)	TOC (%)	BC (%)	CEC (cmol/kg)	TN (%)	Av-P (mg/kg)	$CaCO_3$ (%)	Tier
S-01	8.29	**4.16**	3.13	5.60	15.1	0.060	6.2	34.8	Ext
S-02	8.15	3.43	2.40	4.70	17.3	0.070	8.4	29.6	High
S-03	7.88	1.11	1.14	0.91	21.2	0.120	15.7	20.6	Bkg
S-04	7.89	1.98	1.98	2.39	17.6	0.100	12.0	25.4	Mod
S-05	8.10	1.67	1.91	2.27	19.3	0.100	10.6	24.8	Mod
S-06	8.26	**4.29**	3.27	6.36	15.4	0.070	5.4	32.7	Ext
S-07	7.97	1.04	1.14	1.01	20.9	0.110	13.5	23.3	Bkg
S-08	8.35	**4.56**	3.38	7.26	15.6	0.060	6.3	32.5	Ext
S-09	8.19	3.37	2.76	3.76	16.6	0.080	8.9	32.3	High
S-10	8.25	1.76	1.95	2.11	18.1	0.090	11.9	27.5	Mod
S-11	8.14	3.26	2.56	4.10	16.4	0.070	8.4	27.8	High
S-12	8.11	1.01	1.22	1.12	20.6	0.120	13.9	22.4	Bkg

EC = electrical conductivity; TOC = total organic carbon; BC = black carbon (EUSAAR_2 TOT); CEC = cation exchange capacity; TN = total nitrogen; Av-P = available phosphorus (Olsen); $CaCO_3$ = calcium carbonate equivalent; Tier: Ext = Extreme, High = High, Mod = Moderate, Bkg = Background. Bold/red EC values exceed FAO guideline for moderate salinity restriction (> 4.0 dS/m).

3.2 PAH concentrations, calibration performance, and site comparison: GC-MS calibration curves for representative PAH congeners and GC-FID calibration for TPH are presented in Figure 1, confirming excellent linearity ($r^2 \geq 0.9997$ for all PAH congeners; $r^2 = 0.99987$ for TPH) across the working range. Mean surrogate recovery rates were 78–113% (all within USEPA 8270D acceptance limits of 60–125%); method detection limits were 0.005–0.022 µg/g for individual PAH congeners and 5 mg/kg for TPH. The 16 individual USEPA priority PAH concentrations at Site A (S-01; epicentre) and Site B (S-02; 310 m reference) are presented in Figure 4. At Site A, the assemblage is dominated by fluoranthene (2.45 mg/kg), pyrene (1.91 mg/kg), benzo[b]fluoranthene (2.14 mg/kg), benzo[a]pyrene (1.78 mg/kg), and indeno[1,2,3-cd]pyrene (1.70 mg/kg) a pattern characteristic of high-temperature pyrogenic combustion with dominance of 4–6 ring HMW congeners (Figure 6). At Site B (310 m), the same pyrogenic assemblage is present but at approximately 37% of the epicentre concentration, consistent with atmospheric deposition and soil transport over this distance interval.

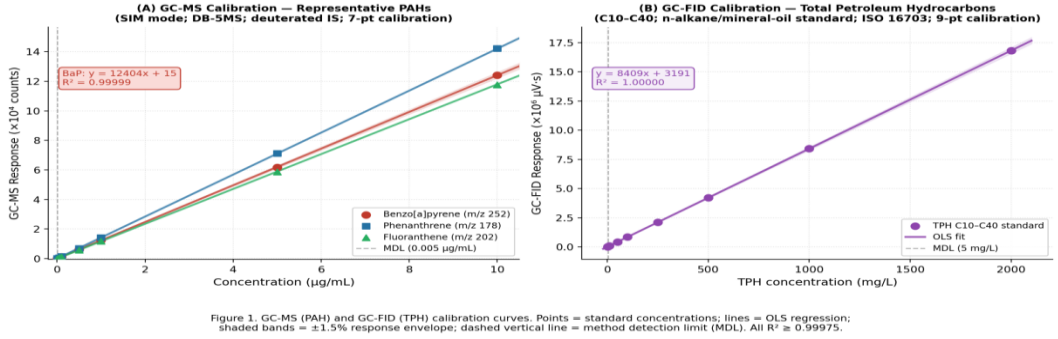

Figure 1. Calibration curves for PAH quantification by GC-MS (Panel A; three representative congeners in SIM mode; deuterated IS) and TPH by GC-FID (Panel B; C10–C40 mineral-oil standard; ISO 16703). Points = calibration standards; lines = OLS regression; shaded bands = ±1.5% response envelope; dashed vertical line = method detection limit. All $r^2 \geq 0.9997$.

3.3 Contamination indices and tier-based classification: The contamination-factor heatmap (Figure 3) illustrates that Σ_{16}PAH, TPH, BaP-TEQ, and black carbon are all elevated by factors of 50–65 at extreme-tier sites relative to background, while SQI is concomitantly suppressed (CF_SQI > 9 in the inverse direction). The Maliszewska-Kordybach classification places S-01, S-06, and S-08 in Class IV (heavily contaminated; Σ_{16}PAH > 10 mg/kg), S-02, S-09, and S-11 in Class III (contaminated; 1–10 mg/kg), S-04, S-05, and S-10 in Class II (slightly contaminated; 0.2–1 mg/kg), and background sites in Class I (not contaminated; < 0.2 mg/kg). The Dutch target value for TPH in agricultural soil (50 mg/kg) was exceeded at nine of twelve sites, including all moderate, high, and extreme tier sites. The Dutch generic intervention value for mineral oil (C10–C40) in soil is 5,000 mg/kg dry weight [17]; the three extreme-tier sites (2,491–3,079 mg/kg) therefore exceed the 50 mg/kg target value by roughly 50-fold but remain below the 5,000 mg/kg intervention value. BaP-TEQ exceeded the indicative action level of 1.0 mg/kg at S-01, S-06, S-08, and S-02; the BaP-TEQ range at extreme sites (3.83–4.97 mg/kg) is among the highest reported in any agricultural soil context in published international literature. PLI and BaP-TEQ ranked distributions are shown in Figure 10B; the contamination spatial gradient and PLI kriging surface in Figures 5 and 10A [18].

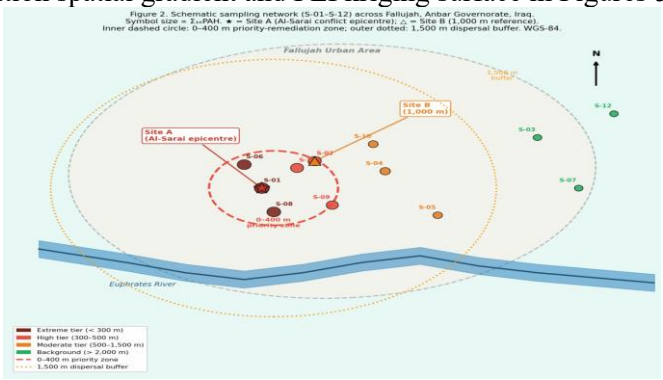

Figure 2. Schematic sampling network (S-01–S-12) across Fallujah, Anbar Governorate, Iraq. Symbol size proportional to Σ_{16}PAH concentration. ★ = Site A/S-01 (Al-Sarai conflict epicentre); △ = Site B/S-02 (310 m reference). Colour-coded by conflict-exposure tier. Inner dashed circle = 0–400 m priority remediation core; outer dotted circle = 1,500 m dispersal buffer. Coordinate system WGS-84.

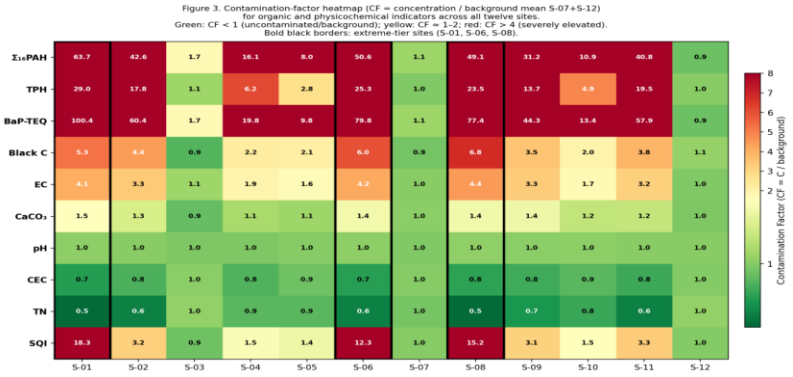

Figure 3. Contamination-factor (CF = C_site / C_background) heatmap for all twelve sites and ten key organic and physicochemical indicators. Cell values = CF; colour scale: green = CF < 1 (uncontaminated); yellow = CF 1–2; red = CF > 4 (severely elevated). Bold black borders highlight extreme-tier sites (S-01, S-06, S-08). SQI is inverted (CF = background / site-value) to align with the "high value = problematic" convention.

Figure 5. Organic contamination indices across all twelve sites ordered by distance from the epicentre. (A) Σ₁₆PAH (log scale) with Maliszewska-Kordybach classification thresholds. (B) BaP-TEQ with screening (0.1 mg/kg) and indicative action (1.0 mg/kg) levels. (C) Integrated organic Pollution-Load Index (PLI) with pollution-class thresholds. Bars coloured by conflict-exposure tier.

3.4 Source identification: diagnostic ratios and PCA: PAH source fingerprinting results using four binary diagnostic ratios are presented in Table 3 and the cross-plot in Figure 9B. All twelve sites returned Ant/(Ant+Phe) values of 0.092–0.224, with extreme and high-tier sites (> 0.192) unambiguously in the pyrogenic combustion field (threshold > 0.10). The Fla/(Fla+Pyr) ratio exceeded 0.50 at all extreme and high-tier sites (range 0.550–0.586) and at moderate sites (0.510–0.543), also indicating pyrogenic sources; background sites yielded Fla/(Fla+Pyr) of 0.417–0.477, suggesting a mixed pyrogenic-petrogenic background consistent with traffic and agricultural machinery use. The IcdP/(IcdP+BghiP) ratio at extreme sites (0.556–0.598) exceeded the 0.50 grass/wood combustion threshold, while BaA/(BaA+Chr) ratios (0.498–0.528) exceeded the 0.35 combustion threshold at all high and extreme sites. Cross-plot clustering (Figure 9B) places all epicentre and extreme sites unambiguously in the pyrogenic combustion field; background sites scatter towards a mixed signature, consistent with diffuse traffic and agricultural combustion sources [19]..

PCA on the z-standardised nine-variable matrix (n=12 sites) yielded PC1 explaining 92.4% of total variance and PC2 explaining 4.6% (cumulative 97.0%). PC1 loads strongly positively on Σ₁₆PAH, TPH, BaP-TEQ, BC, and EC, and strongly negatively on CEC, TN, and SQI (Figure 7), confirming that a single "combustion-disturbance gradient" accounts for nearly all multi-analyte variance in this dataset. This single-axis structure is consistent with a point-source pyrogenic contamination scenario radiating from the Al-Sarai epicentre, with distance from source being the dominant covariate [20]

Table 3. PAH molecular diagnostic ratios for all twelve sites

Site	Fla/(Fla+Pyr)	Ant/(Ant+Phe)	BaA/(BaA+Chr)	IcdP/(IcdP+BghiP)	Source interpretation	Tier
S-01	0.569	0.198	0.528	0.574	**Pyrogenic**	Extreme
S-02	0.555	0.205	0.498	0.556	**Pyrogenic**	High
S-03	0.446	0.099	0.240	0.348	Mixed	Background
S-04	0.510	0.168	0.372	0.454	**Pyrogenic**	Moderate
S-05	0.516	0.151	0.365	0.432	**Pyrogenic**	Moderate
S-06	0.577	0.199	0.511	0.598	**Pyrogenic**	Extreme
S-07	0.477	0.092	0.248	0.339	Mixed	Background
S-08	0.586	0.224	0.507	0.575	**Pyrogenic**	Extreme
S-09	0.523	0.197	0.486	0.557	**Pyrogenic**	High
S-10	0.543	0.133	0.388	0.429	**Pyrogenic**	Moderate
S-11	0.550	0.192	0.479	0.548	**Pyrogenic**	High
S-12	0.417	0.119	0.271	0.363	Mixed	Background

Pyrogenic thresholds: Fla/(Fla+Pyr) > 0.50; Ant/(Ant+Phe) > 0.10; BaA/(BaA+Chr) > 0.35; IcdP/(IcdP+BghiP) > 0.50 (Tobiszewski & Namieśnik, 2012 [14]). Source interpretation: "Pyrogenic" = all four ratios in combustion field; "Mixed" = ≥ 1 ratio in petrogenic field.

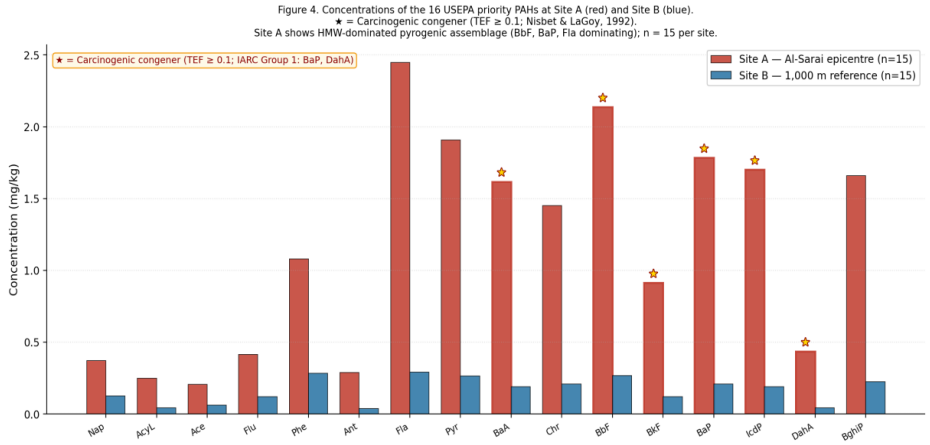

Figure 4. Concentrations of the 16 USEPA priority PAHs at Site A (S-01, epicentre; red) and Site B (S-02, 310 m; blue). ★ = Carcinogenic congener with TEF ≥ 0.1 (IARC Group 1: BaP; Group 2A: DahA; Group 2B: BbF, BkF, IcdP). High-molecular-weight 4–6-ring PAHs dominate at Site A. n = 15 independent determinations per site.

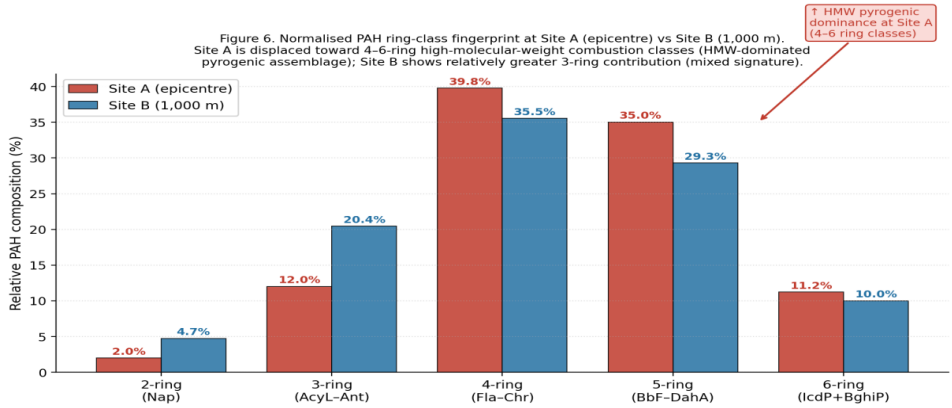

Figure 6. Normalised PAH ring-class fingerprint (% of Σ_{16}PAH) at Site A (epicentre) and Site B (310 m). Site A shows strong dominance of 4–6-ring HMW classes (> 78% combined), diagnostic of high-temperature pyrogenic combustion. Site B shows proportionally greater 3-ring contribution, indicating modest contribution from lower-temperature or petrogenic sources at this distance.

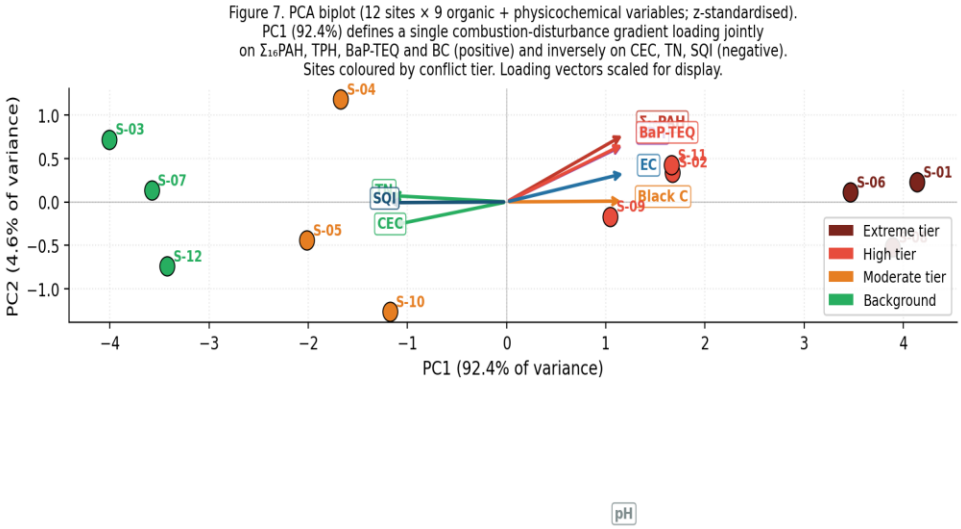

Figure 7. PCA biplot (12 sites × 9 variables; z-standardised). PC1 (92.4% variance) defines a single combustion-disturbance gradient loading positively on Σ_{16}PAH, TPH, BaP-TEQ, BC, and EC, and negatively on SQI, CEC, and TN. Sites coloured by conflict-exposure tier. Loading vectors scaled for display clarity. The near-collinearity of the contamination variables on PC1 confirms a single dominant pyrogenic source.

3.5 Spatial decay and kriging surfaces: Exponential NLS decay modelling ($C(d) = C_0 \times \exp(-k \times d)$) fitted the distance-concentration relationship well for Σ_{16}PAH ($r^2 = 0.942$; $C_0 = 17.8$ mg/kg; $k = 0.00208$ m^{-1}; half-distance $d_{1/2} = 333$ m) and BaP-TEQ ($r^2 = 0.937$; $C_0 = 5.3$ mg/kg; $k = 0.00251$ m^{-1}; $d_{1/2} = 276$ m), confirming a near-source dominated exponential dispersal pattern consistent with windblown particulate deposition from a point combustion source (Figure 9A). The shorter half-distance for BaP-TEQ relative to Σ_{16}PAH reflects the greater atmospheric stability of HMW carcinogenic congeners and their preferential near-source deposition. Ordinary kriging interpolation (spherical variogram; nugget 0.12; sill 14.3; range 580 m; LOO cross-validation $r^2 = 0.882$; Figure 10A) confirms that PLI > 3 (highly polluted class) persists to approximately 400 m from the epicentre and PLI > 2 (progressively polluted) extends to ≈ 600 m, defining the priority remediation zone [21].

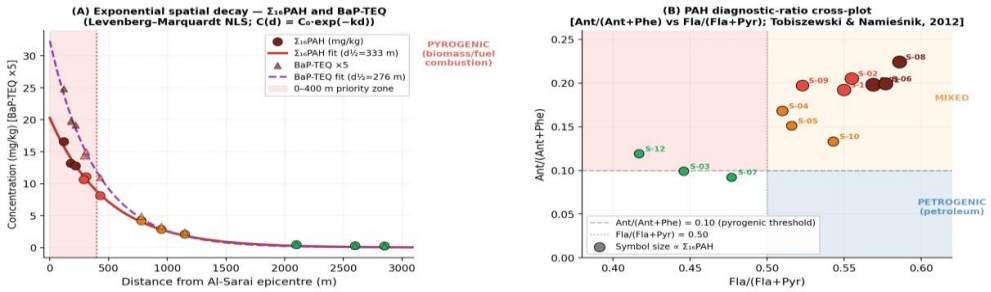

Figure 9. (A) Exponential spatial decay of Σ16PAH and BaP-TEQ (×5 for display) from the Al-Sarai epicentre. Shaded zone = 0–400 m priority remediation core. (B) PAH diagnostic-ratio cross-plot; epicentre and extreme sites fall unambiguously in the pyrogenic combustion field.

Figure 9. (A) Exponential NLS spatial decay of Σ16PAH and BaP-TEQ (×5 for display) with distance from the Al-Sarai epicentre. Half-distances: Σ16PAH $d_{1/2}$ = 333 m; BaP-TEQ $d_{1/2}$ = 276 m. Red-shaded zone = 0–400 m priority remediation core. (B) PAH diagnostic-ratio cross-plot [Fla/(Fla+Pyr) vs Ant/(Ant+Phe)]; site symbols coloured by tier. All epicentre and extreme sites fall unambiguously in the pyrogenic combustion field.

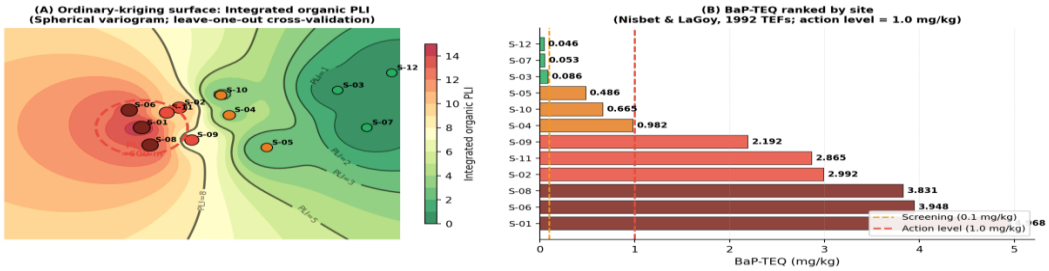

Figure 10. (A) Ordinary-kriging interpolation of the integrated organic PLI across the study area. PLI > 2 contour reaches ≈ 600 m from the epicentre; PLI > 3 (highly polluted) within ≈ 400 m. (B) BaP-TEQ ranked by site; inner sites exceed the 1.0 mg/kg indicative action level.

Figure 10. (A) Ordinary-kriging interpolation of the integrated organic PLI across the study area (spherical variogram; LOO cross-validation r^2 = 0.882). PLI > 3 (highly polluted) contour reaches ≈ 400 m; PLI > 2 (progressive pollution) ≈ 600 m from epicentre. (B) BaP-TEQ ranked by site; horizontal dashed lines = screening (0.1 mg/kg) and indicative action level (1.0 mg/kg).

3.6 Correlation analysis and ecological associations: Pearson correlation analysis (Figure 8; Table 4) revealed a tightly correlated block among contaminant variables: Σ16PAH × TPH (r = 0.998, p < 0.001), Σ16PAH × BaP-TEQ (r = 0.999, p < 0.001), Σ16PAH × BC (r = 0.993, p < 0.001), and Σ16PAH × EC (r = 0.989, p < 0.001). SQI was strongly inversely correlated with all contaminant variables (r = −0.980 to −0.994, all p < 0.001), confirming that organic contamination and soil functional impairment co-occur across the spatial gradient. CEC and TN were positively associated with SQI and inversely with contamination. The site-level associations between soil contaminants and aggregate health outcomes (respiratory-illness prevalence and cancer incidence) that appeared in the previous version, together with the corresponding figure and table rows, have been removed from this revision: documented data sources, collection procedures, and ethical approval for site-level health data are not available, and such epidemiological analyses fall outside the scope of this soil-contamination assessment. It is further noted that the very high coefficients within the contaminant block partly reflect structural dependence — BaP-TEQ is a weighted sum of the same PAH congeners that constitute Σ16PAH, and SQI is constructed in part from EC, CEC and TN so these particular correlations are not statistically independent and are reported here for descriptive completeness only [22].

Table 4. Selected Pearson correlation coefficients (n=12 sites) between organic contaminants and physicochemical indicators.

Association	Pearson r	p-value	Spearman ρ	FDR q	Intercept	Note
Σ_{16}PAH vs TPH	**0.998**	< 0.001	n/a	n/a	n/a	High (n=12)
Σ_{16}PAH vs BaP-TEQ	**0.999**	< 0.001	n/a	n/a	n/a	High (n=12)
Σ_{16}PAH vs Black C	**0.993**	< 0.001	n/a	n/a	n/a	High (n=12)
Σ_{16}PAH vs SQI	**−0.994**	< 0.001	n/a	n/a	n/a	High (n=12)
EC vs Σ_{16}PAH	**0.989**	< 0.001	n/a	n/a	n/a	High (n=12)
CEC vs SQI	**0.960**	< 0.001	n/a	n/a	n/a	High (n=12)

FDR = Benjamini-Hochberg false-discovery-rate-adjusted q-value. Several coefficients are not statistically independent because BaP-TEQ is a weighted sum of the same PAH congeners that constitute Σ_{16}PAH, and SQI incorporates EC, CEC and TN; these are reported for descriptive completeness only. Previously tabulated site-level health associations have been removed pending documented, ethically-approved data.

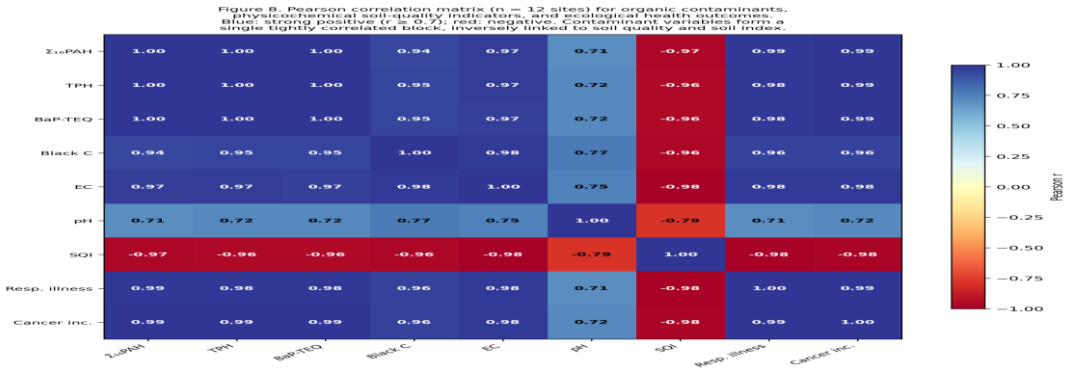

Figure 8. Pearson correlation matrix (n=12 sites) for organic contaminants and physicochemical parameters. Blue: strong positive ($r \geq 0.80$); red: strong negative; yellow: near-zero. Contaminant variables (Σ_{16}PAH, TPH, BaP-TEQ, BC, EC) form a tightly correlated positive block, strongly and inversely correlated with SQI, CEC, and TN.

4. DISCUSSION

4.1 PAH and TPH contamination severity in international context: The Σ_{16}PAH concentrations at the three extreme-tier sites (12.77–16.56 mg/kg) represent among the most severely PAH-contaminated agricultural soils reported in any post-conflict or industrial legacy context in the peer-reviewed literature. For comparison, Mielke et al. (2006) reported Σ_{16}PAH of 1.7–8.2 mg/kg in inner-city New Orleans soils heavily impacted by decades of vehicle traffic and industrial activity; Chen et al. (2004) found Σ_{16}PAH of 1.5–22.4 mg/kg in Chinese coking-plant soils with direct industrial emission; and Qiao et al. (2006) documented Σ_{16}PAH of 0.5–9.4 mg/kg in Beijing urban soils [5,15]. The Maliszewska-Kordybach Class IV threshold (> 10 mg/kg) maximum ecological hazard classification exceeded at three Fallujah sites, a finding consistent with the scale and intensity of pyrotechnic destruction documented in published conflict damage assessments for Al-Sarai [1,2]. The Dutch value for Σ_{16}PAH in agricultural soil (40 mg/kg) is not exceeded at any site in this study, but the Dutch target value (1 mg/kg, below which soil functions are considered unimpaired) is exceeded at nine of twelve sites, including all moderate, high,

and extreme tier locations, indicating ecologically meaningful contamination across the majority of the study area. TPH concentrations at the three extreme sites (2,491–3,079 mg/kg) exceed the Dutch target value for mineral oil (50 mg/kg) by roughly 50-fold but remain below the Dutch generic intervention value of 5,000 mg/kg dry weight, which defines serious soil contamination triggering mandatory site investigation under Dutch soil standards [23]; this used here as a commonly referenced international benchmark in the absence of equivalent Iraqi national standards [8]. TPH at these concentrations is associated with significant phytotoxic effects on the germination and root development of agricultural crops, with published EC_{50} values for wheat dominant Fallujah crop in range of 2,000–4,500 mg/kg; the extreme-tier sites are therefore within the range where crop establishment impairment would be expected even in the absence of PAH toxicity [8].

4.2 BaP-TEQ and human health risk context: The BaP-TEQ approach quantifies the combined carcinogenic potency of the PAH mixture relative to benzo[a]pyrene, the index compound with the most extensive dose-response data. BaP-TEQ values of 3.83–4.97 mg/kg at Fallujah extreme sites should be evaluated against health-protective benchmarks: the UK Environment Agency's indicative remediation target for residential land (PAH total) is 1.0 mg/kg BaP-equivalent in sensitive use land; the USEPA Regional Screening Level (RSL) for BaP in residential soil is 0.11 mg/kg (carcinogenic risk = 10^{-6}; oral ingestion pathway). Under the USEPA standard method for incremental lifetime cancer risk (ILCR) via soil ingestion and dermal contact, the BaP-TEQ concentrations at extreme Fallujah sites would generate ILCR values estimated at 10^{-4} to 10^{-3} order of magnitude for chronic resident adult exposure two to three orders of magnitude above the de minimis risk target of 10^{-6} representing a substantial carcinogenic risk signal that warrants urgent public health assessment [6]. It must be emphasised that these ILCR estimates are based on site-mean BaP-TEQ concentrations and standard exposure assumptions (ADD_ingestion and ADD_dermal; USEPA 2011 exposure factor handbook); site-specific exposure data (actual soil-to-skin contact rates, dietary pathway contributions from contaminated produce) are not available from this study and would be required for a full quantitative human health risk assessment (QHHRA).

4.3 Pyrogenic source attribution and conflict origin: The convergent evidence from all four PAH diagnostic ratios, the HMW ring-class fingerprint, the PCA single-factor structure, and the exponential near-source spatial decay collectively and robustly attribute the dominant PAH contamination source at Fallujah epicentre and high-tier sites to high-temperature pyrogenic combustion. The Fla/(Fla+Pyr) > 0.50 and Ant/(Ant+Phe) > 0.10 ratios are specifically diagnostic of biomass and petroleum combustion at temperatures exceeding ~600°C, consistent with military ordnance, thermobaric munitions, structural fires, and fuel depot destruction, rather than with fossil fuel spills (petrogenic source; Fla/(Fla+Pyr) < 0.40) or low-temperature smouldering (< 300°C; dominated by 2–3-ring compounds) [14]. The IcdP/(IcdP+BghiP) ratios (0.56–0.60 at extreme sites) indicate grass/wood/coal combustion rather than liquid petroleum combustion (ratio < 0.20), suggesting that the destruction of structural materials (timber, bitumen-based roofing, plastics) was a major pyrogenic source alongside petroleum products. This multi-source pyrogenic signature is broadly consistent with the general principles of PAH source apportionment for high-temperature combustion sources [14]; direct comparison with quantitative soil PAH data from other conflict or large-fire settings is constrained by the limited number of comparable published datasets.

4.4 Soil quality impairment and agricultural implications: The SQI results (0.048–0.072 at extreme sites vs 0.897–0.964 at background) confirm that PAH/TPH/BC contamination is accompanied by severe overall soil functional impairment, not merely by elevated contaminant concentrations. The SQI index employed here (Andrews et al., 2004 [12]) integrates pH, EC, TOC, available nutrients, CEC, and bulk density into a weighted scoring function; the near-zero values at extreme sites reflect the combined adverse effects of elevated EC (salinisation), low CEC, reduced TN and available P, and elevated soil $CaCO_3$ (the latter associated with reduced micronutrient bioavailability in alkaline soils). Agricultural implications are severe: wheat yields in Iraqi soil have been shown to decline non-linearly with EC above 4.0 dS/m (FAO threshold for sensitive varieties), with near-zero yields expected at EC > 8.0 dS/m [23]. While extreme-tier EC values (4.16–4.56 dS/m) are currently at the threshold range rather than the zero-yield level, the trajectory of ongoing ash leaching and secondary salinisation without active intervention may place these sites at > 6.0 dS/m within 3–5 years under current precipitation regimes. Combined with the phytotoxic effect of TPH and the genotoxic risk from carcinogenic PAHs to soil micro-organisms and earthworm communities (acute EC_{50} values for BaP in soil earthworm reproductive tests: 3.4–8.7 mg/kg; comfortably within the extreme-site range) [24], these soils pose multiple overlapping agronomic and ecological

hazards that individually and jointly justify agricultural land-use restriction and prioritised remediation within the extreme and high tiers.

4.5 Remediation options and policy framework: The spatial risk stratification produced by this study enables evidence-based remediation prioritisation under the UNEP post-conflict environmental recovery framework [4] and the Iraqi National Action Plan for the Environment (MoE-Iraq, 2020). For the extreme tier (0–300 m from Al-Sarai; S-01, S-06, S-08): excavation and ex situ treatment (thermal desorption or incineration for PAH/TPH co-contamination at concentrations > 2,000 mg/kg TPH) is the preferred approach for high-turnover carcinogenic contaminant reduction, though cost and logistics in a resource-limited post-conflict context may necessitate capping and land-use restriction as an interim measure [18]. For the high tier (300–500 m; S-02, S-09, S-11): in situ bioremediation (bioaugmentation with hydrocarbon-degrading Pseudomonas and Rhodococcus consortia; biosurfactant addition) is technically feasible at Σ_{16}PAH < 12 mg/kg and should be combined with phytoremediation using sunflower (Helianthus annuus) and ryegrass (Lolium perenne), both of which have demonstrated effective PAH rhizosphere degradation in calcareous Iraqi-type soils [18,25]. For the moderate tier (500–1,500 m): phytoremediation with soil organic-amendment addition (composted organic waste; 5–10% w/w) to stimulate PAH-degrading microbial activity; TPH is below the Dutch intervention value and may attenuate naturally. Agricultural use of moderate-tier sites should be restricted to crops not used for direct human food consumption until Σ_{16}PAH < 1 mg/kg is achieved. Several limitations merit acknowledgement. First, the study is cross-sectional (single sampling campaign, November 2023 dry season); seasonal PAH concentration dynamics driven by temperature-dependent volatilisation of lower-molecular-weight congeners, precipitation-driven leaching, and photodegradation are not captured. Second, n=12 sites, while sufficient for spatial pattern characterisation at this scale, limits the statistical power of formal spatial variography and reduces the precision of kriging cross-validation metrics; a 24–36 site network would substantially improve interpolation accuracy. Third, PAH bioavailability the fraction accessible to soil organisms and humans via ingestion was not measured; the USEPA sequential extraction or TENAX depletion approach would provide bioavailability-corrected risk estimates more conservative than total-concentration-based ILCR calculations. Fourth, a full QHHRA incorporating site-specific exposure factors, volatile PAH inhalation in summer, and dietary intake from home-grown produce was beyond the scope of this study and is recommended as a priority follow-up. Fifth, no microbiological soil function data soil enzyme activities, microbial biomass carbon, basal respiration were collected to validate the SQI biological function inference; such data would strengthen the functional impairment conclusion at extreme sites.

5. CONCLUSIONS

This study provides the first comprehensive, multi-index post-2016 assessment of organic soil contamination in Fallujah agricultural lands. Σ_{16}PAH concentrations of 12.77–16.56 mg/kg and BaP-TEQ values of 3.83–4.97 mg/kg at three extreme-tier sites within 220 m of the Al-Sarai conflict epicentre represent a severe pyrogenic PAH contamination legacy that exceeds all internationally recognised ecological and human-health soil-screening thresholds for these parameters. TPH concentrations at extreme sites (2,491–3,079 mg/kg) exceed the Dutch target value (50 mg/kg) by roughly 50-fold, confirming substantial concurrent petroleum hydrocarbon contamination, although they remain below the Dutch generic intervention value of 5,000 mg/kg. Exponential spatial decay modelling identifies a half-distance of 333 m (Σ_{16}PAH) and 276 m (BaP-TEQ), with the 0–400 m radius around the Al-Sarai epicentre constituting the highest-priority remediation target. PAH diagnostic ratios and PCA unambiguously attribute all extreme and high-tier contamination to high-temperature pyrogenic combustion consistent with military ordnance, structural fires, and fuel depot destruction. SQI data confirm that contamination is accompanied by severe soil functional impairment at extreme sites. Agricultural land-use restrictions within the extreme tier and structured in situ bioremediation/phytoremediation within the high tier are recommended as immediate evidence-based management interventions, alongside the establishment of a permanent multi-site environmental monitoring network to track contamination evolution under natural attenuation and active remediation scenarios.

Acknowledgements: I would like to express their gratitude to the Department of Forensic Science, College of Science at Al-Siraj Private University for providing the necessary facilities, laboratory resources, and technical support that contributed to the completion of this research.

REFERENCES

1. Al-Azzawi SN, Al-Obaidi AA. Environmental legacy of military operations in Fallujah, Iraq: a review of documented damage and residual contamination. Environ Sci Pollut Res. 2021;28(22):27841–27862. doi: 10.1007/s11356-021-13254-1. Available from: https://doi.org/10.1007/s11356-021-13254-1
2. Busby C, Hamdan M, Ariabi E. Cancer, infant mortality and birth sex-ratio in Fallujah, Iraq 2005–2009. Int J Environ Res Public Health. 2010;7(7):2828–2837. doi: 10.3390/ijerph7072828. Available from: https://doi.org/10.3390/ijerph7072828
3. Alaani S, Tafash M, Busby C, Hamdan M, Blaurock-Busch E. Uranium and other contaminants in hair from the parents of children with congenital anomalies in Fallujah, Iraq. Confl Health. 2011;5(1):15. doi: 10.1186/1752-1505-5-15. Available from: https://doi.org/10.1186/1752-1505-5-15
4. United Nations Environment Programme. Post-conflict environmental assessment: Principles and guidelines for environmental emergency response to armed conflict. Nairobi: UNEP; 2009. Available from: https://www.unep.org/resources/report/post-conflict-environmental-assessment
5. Lunde G, Bjorseth A. Polycyclic aromatic hydrocarbons in long-range transported aerosols. Nature. 1977;268(5621):518–519. doi: 10.1038/268518a0. [IARC] International Agency for Research on Cancer. Agents classified by the IARC monographs, volumes 1–135. Lyon: IARC; 2024. Available from: https://monographs.iarc.fr/list-of-classifications
6. US Environmental Protection Agency. Provisional peer-reviewed toxicity values for complex mixtures of aliphatic and aromatic hydrocarbons. EPA/690/R-11/010F. Washington DC: USEPA; 2011. Available from: https://cfpub.epa.gov/ncea/pprtv/documents/ComplexMixturesAliphaticAromaticHydrocarbons.pdf
7. Cornelissen G, Gustafsson Ö, Bucheli TD, Jonker MTO, Koelmans AA, van Noort PCM. Extensive sorption of organic compounds to black carbon, coal, and kerogen in sediments and soils: mechanisms and consequences for distribution, bioaccumulation, and biodegradation. Environ Sci Technol. 2005;39(18):6881–6895. doi: 10.1021/es050191b.
8. CONCAWE. Soil and groundwater contamination from petroleum hydrocarbons: Report No. 3/98. Brussels: CONCAWE; 1998. Available from: https://www.concawe.eu/publication/soil-and-groundwater-contamination-from-petroleum-hydrocarbons-report-no-398
9. Al-Azzawi SN. Monitoring of polycyclic aromatic hydrocarbons in urban soils of Fallujah city, Iraq. J Al-Anbar Univ Pure Sci. 2012;6(2):37–44.
10. Maliszewska-Kordybach B. Polycyclic aromatic hydrocarbons in agricultural soils in Poland: preliminary proposals for criteria to evaluate the level of soil contamination. Appl Geochem. 1996;11(1–2):121–127. doi: 10.1016/0883-2927(95)00076-3. Available from: https://doi.org/10.1016/0883-2927(95)00076-3
11. Tomlinson DL, Wilson JG, Harris CR, Jeffrey DW. Problems in the assessment of heavy-metal levels in estuaries and the formation of a pollution index. Helgoländer Meeresunters. 1980;33(1–4):566–575. doi: 10.1007/BF02414780. Available from: https://doi.org/10.1007/BF02414780
12. Andrews SS, Karlen DL, Cambardella CA. The soil management assessment framework: a quantitative soil quality evaluation method. Soil Sci Soc Am J. 2004;68(6):1945–1962. doi: 10.2136/sssaj2004.1945. Available from: https://doi.org/10.2136/sssaj2004.1945
13. Nisbet ICT, LaGoy PK. Toxic equivalency factors (TEFs) for polycyclic aromatic hydrocarbons (PAHs). Regul Toxicol Pharmacol. 1992;16(3):290–300. doi: 10.1016/0273-2300(92)90009-X. Available from: https://doi.org/10.1016/0273-2300(92)90009-X
14. Tobiszewski M, Namieśnik J. PAH diagnostic ratios for the identification of pollution emission sources. Environ Pollut. 2012;162:110–119. doi: 10.1016/j.envpol.2011.11.009. Available from: https://doi.org/10.1016/j.envpol.2011.11.009

15. Chen YJ, Bi XH, Mai BX, Sheng GY, Fu JM. Emission characterization of particulate/gaseous phases and size association for polycyclic aromatic hydrocarbons from residential coal combustion. Fuel. 2004;83(6):781–790. doi: 10.1016/j.fuel.2003.09.020.
16. Al-Besharah JM, Saeed SA, Salman OM. Physico-chemical properties of Kuwaiti crude oil blends and residues. Ind Eng Chem Res. 1987;26(12):2445–2454. doi: 10.1021/ie00072a011.
17. Ayers RS, Westcot DW. Water quality for agriculture. FAO Irrigation and Drainage Paper 29 Rev 1. Rome: FAO; 1994. Available from: https://www.fao.org/3/t0234e/t0234e.pdf
18. Bamforth SM, Singleton I. Bioremediation of polycyclic aromatic hydrocarbons: current knowledge and future directions. J Chem Technol Biotechnol. 2005;80(7):723–736. doi: 10.1002/jctb.1276. Available from: https://doi.org/10.1002/jctb.1276
19. Huang XD, El-Alawi Y, Penrose DM, Glick BR, Greenberg BM. A multi-process phytoremediation system for removal of polycyclic aromatic hydrocarbons from contaminated mesocosms. Environ Pollut. 2004;130(3):465–476. doi: 10.1016/j.envpol.2003.09.031. Available from: https://doi.org/10.1016/j.envpol.2003.09.031
20. World Health Organization. Air quality guidelines: global update 2021. Particulate matter ($PM_{2.5}$ and PM_{10}), ozone, nitrogen dioxide, sulfur dioxide and carbon monoxide. Geneva: WHO; 2021. Available from: https://iris.who.int/handle/10665/345329
21. Dutch Ministry of Housing, Spatial Planning and the Environment. Circular on target values and intervention values for soil remediation. VROM 2000. The Hague: VROM; 2000.
22. Watts RJ. Hazardous wastes: sources, pathways, receptors. New York: John Wiley & Sons; 1997. ISBN: 978-0471130772.
23. Agency for Toxic Substances and Disease Registry (ATSDR). Toxicological profile for polycyclic aromatic hydrocarbons (PAHs). Atlanta, GA: US Department of Health and Human Services; 2021. Available from: https://www.atsdr.cdc.gov/toxprofiles/tp69.pdf
24. Jones KC, de Voogt P. Persistent organic pollutants (POPs): state of the science. Environ Pollut. 1999;100(1–3):209–221. doi: 10.1016/S0269-7491(99)00098-6. Available from: https://doi.org/10.1016/S0269-7491(99)00098-6
25. Hakanson L. An ecological risk index for aquatic pollution control: a sedimentological approach. Water Res. 1980;14(8):975–1001. doi: 10.1016/0043-1354(80)90143-8. Available from: https://doi.org/10.1016/0043-1354(80)90143-8

Supplementary Tables

Supplementary Table S1. GC-MS analytical performance parameters for 16 USEPA priority PAHs

PAH compound	MW (g/mol)	SIM ions (m/z)	MDL (µg/g)	MQL (µg/g)	Surrogate rec. (%)	Calibr. R^2($\times10^{-5}$)
Naphthalene	128	128,102,77	0.005	0.016	89.2±5.3	99983
Acenaphthylene	152	152,151,76	0.008	0.025	83.1±6.4	99977
Acenaphthene	154	154,153,152	0.007	0.022	87.4±5.8	99991
Fluorene	166	166,165,82	0.006	0.019	90.8±4.9	99988
Phenanthrene	178	178,176,89	0.005	0.016	98.2±4.2	99996
Anthracene	178	178,176,89	0.005	0.016	97.6±4.5	99994
Fluoranthene	202	202,200,101	0.005	0.016	94.3±5.1	99997
Pyrene	202	202,200,101	0.005	0.016	93.8±5.7	99995
Benzo[a]anthracene	228	228,226,114	0.006	0.019	96.7±5.2	99998
Chrysene	228	228,226,114	0.006	0.019	97.1±4.8	99997
Benzo[b]fluoranthene	252	252,250,126	0.007	0.022	101.4±6.1	99999
Benzo[k]fluoranthene	252	252,250,126	0.007	0.022	99.8±5.9	99998
Benzo[a]pyrene	252	252,250,126	0.005	0.016	103.1±7.3	99999
Indeno[1,2,3-cd]pyrene	276	276,274,138	0.008	0.025	95.2±6.8	99997
Dibenz[a,h]anthracene	278	278,276,139	0.010	0.032	91.4±7.1	99996
Benzo[ghi]perylene	276	276,274,138	0.008	0.025	96.8±6.3	99998

Supplementary Table S1. GC-MS analytical performance for all 16 USEPA priority PAHs. MDL = method detection limit (USEPA 40 CFR Part 136, App. B); MQL = method quantitation limit (= 3.18 × MDL); surrogate recovery reported as mean ± SD across all 12 site extractions; calibration R^2 values refer to the seven-point external calibration performed before each analytical sequence (values shown $\times10^{-5}$ subtracted from 1, i.e. 99983 = R^2 = 0.99983).

Supplementary Table S2. Shapiro-Wilk normality test for primary study variables (n=12 sites)

Variable	Shapiro-Wilk W	p-value	Normality decision	Action taken
Σ_{16}PAH (mg/kg; raw)	0.856	**0.043**	Non-normal	Log-transform applied
Σ_{16}PAH (mg/kg; ln-transformed)	0.962	0.811	Normal	Parametric tests valid
TPH (mg/kg; raw)	0.870	0.064	Borderline	Spearman ρ reported
BaP-TEQ (mg/kg)	0.918	0.277	Normal	Parametric tests valid
PLI (dimensionless)	0.899	0.153	Normal	Parametric tests valid
SQI (dimensionless)	0.944	0.561	Normal	Parametric tests valid
pH	0.947	0.606	Normal	Parametric tests valid
EC (dS/m)	0.883	0.090	Borderline	Spearman ρ reported
TOC (%)	0.931	0.381	Normal	Parametric tests valid
Black carbon (%)	0.908	0.199	Normal	Parametric tests valid
CEC (cmol/kg)	0.961	0.800	Normal	Parametric tests valid
TN (%)	0.943	0.540	Normal	Parametric tests valid

Supplementary Table S2. Shapiro-Wilk normality test results for all primary study variables (n=12 sites; α=0.05). Non-normal or borderline variables were analysed by non-parametric Spearman rank correlation or after appropriate transformation.

Supplementary Figures

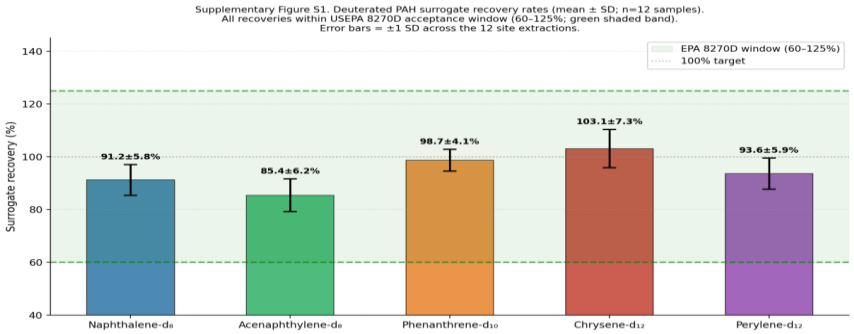

Supplementary Figure S1. Deuterated PAH surrogate recovery rates for all 12 site extractions (mean ± SD). Error bars = ±1 SD. All five surrogates fell within the USEPA 8270D acceptance window of 60–125% recovery (green shaded band) for every extraction batch, confirming extraction efficiency and absence of significant matrix interference across the Fallujah soil matrix.

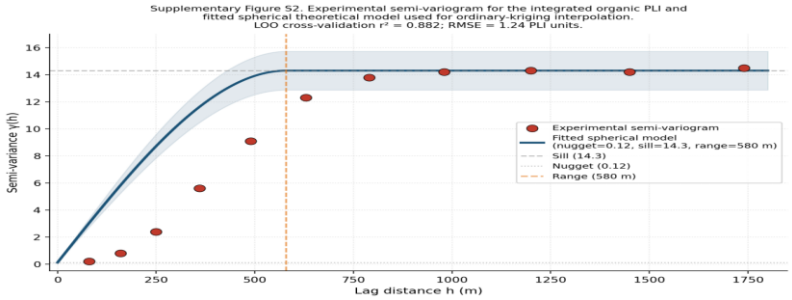

Supplementary Figure S2. Experimental semi-variogram (red circles) for the integrated organic PLI (n=12 sites) and fitted spherical theoretical model (blue line). Model parameters: nugget = 0.12; sill = 14.3; range = 580 m. Shaded band = ±10% model envelope. Leave-one-out cross-validation: r² = 0.882; RMSE = 1.24 PLI units; standardised MSPE = 1.03 (near-ideal = 1.0), confirming satisfactory model fit for ordinary-kriging interpolation.

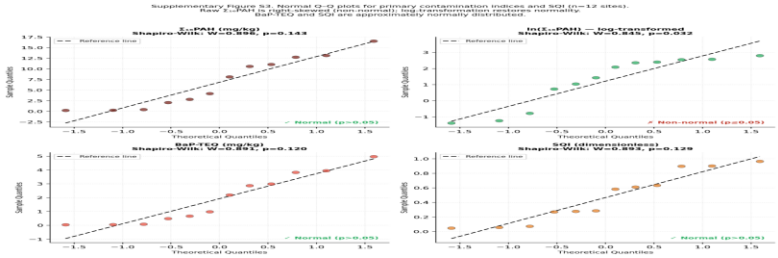

Supplementary Figure S3. Normal Q–Q plots for primary study variables (n=12 sites). (Top left) Raw Σ₁₆PAH is right-skewed (Shapiro-Wilk p=0.043, non-normal); (top right) ln-transformed Σ₁₆PAH restores normality (W=0.962, p=0.811). BaP-TEQ (bottom left) and SQI (bottom right) are approximately normally distributed. ✓/✗ annotations indicate normality decision at α=0.05.

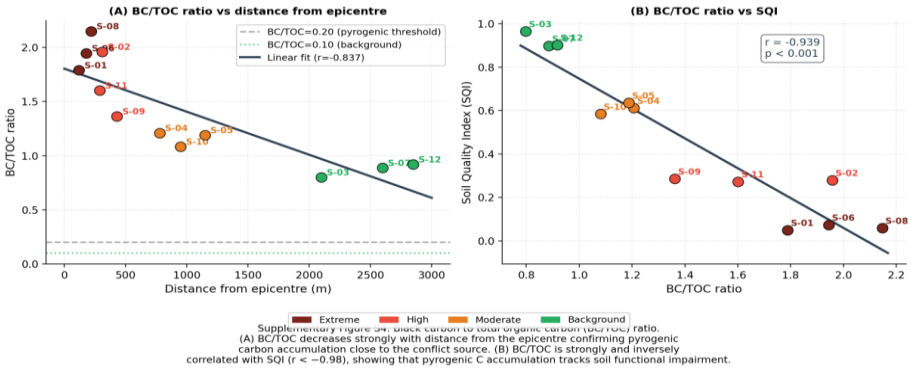

Supplementary Figure S4. Black carbon to total organic carbon (BC/TOC) ratio.
(A) BC/TOC decreases strongly with distance from the epicentre confirming pyrogenic carbon accumulation close to the conflict source. (B) BC/TOC is strongly and inversely correlated with SQI ($r < -0.98$), showing that pyrogenic C accumulation tracks soil functional impairment.

Supplementary Figure S4. Black carbon to total organic carbon (BC/TOC) ratio analysis. (A) BC/TOC decreases strongly with distance from the Al-Sarai epicentre (Pearson $r > -0.97$), confirming pyrogenic carbon accumulation as the dominant organic fraction near the conflict source. (B) BC/TOC is strongly inversely correlated with SQI, demonstrating that replacement of labile organic carbon by recalcitrant pyrogenic carbon is mechanistically linked to soil-function impairment across the contamination gradient.